ACS APPLIED MATERIALS & INTERFACES

Research Article

www.acsami.org

# Relevance of $LiPF_6$ as Etching Agent of $LiMnPO_4$ Colloidal Nanocrystals for High Rate Performing Li-ion Battery Cathodes

Lin Chen,[†] Enrico Dilena,[†] Andrea Paolella,[§] Giovanni Bertoni,[†,∥] Alberto Ansaldo,[‡] Massimo Colombo,[†] Sergio Marras,[†] Bruno Scrosati,[†] Liberato Manna,*[,†] and Simone Monaco*[,†]

[†]Department of Nanochemistry, and [‡]Graphene Laboratories, Istituto Italiano di Tecnologia, via Morego 30, 16163 Genova, Italy

[§]IREQ - Institut de Recherche d'Hydro-Québec, 1800 Boulevard Lionel Boulet, Varennes, QC J3X 1S, Canada

[∥]IMEM-CNR, Parco Area delle Scienze 37/A, 43124 Parma, Italy

Supporting Information

**ABSTRACT:** $LiMnPO_4$ is an attractive cathode material for the next-generation high power Li-ion batteries, due to its high theoretical specific capacity (170 mA h $g^{-1}$) and working voltage (4.1 V vs $Li^+$/Li). However, two main drawbacks prevent the practical use of $LiMnPO_4$: its low electronic conductivity and the limited lithium diffusion rate, which are responsible for the poor rate capability of the cathode. The electronic resistance is usually lowered by coating the particles with carbon, while the use of nanosize particles can alleviate the issues associated with poor ionic conductivity. It is therefore of primary importance to develop a synthetic route to $LiMnPO_4$ nanocrystals (NCs) with controlled size and coated with a highly conductive carbon layer. We report here an effective surface etching process (using $LiPF_6$) on colloidally synthesized $LiMnPO_4$ NCs that makes the NCs dispersible in the aqueous glucose solution used as carbon source for the carbon coating step. Also, it is likely that the improved exposure of the NC surface to glucose facilitates the formation of a conductive carbon layer that is in intimate contact with the inorganic core, resulting in a high electronic conductivity of the electrode, as observed by us. The carbon coated etched $LiMnPO_4$-based electrode exhibited a specific capacity of 118 mA h $g^{-1}$ at 1C, with a stable cycling performance and a capacity retention of 92% after 120 cycles at different C-rates. The delivered capacities were higher than those of electrodes based on not etched carbon coated NCs, which never exceeded 30 mA h $g^{-1}$. The rate capability here reported for the carbon coated etched $LiMnPO_4$ nanocrystals represents an important result, taking into account that in the electrode formulation 80% wt is made of the active material and the adopted charge protocol is based on reasonable fast charge times.

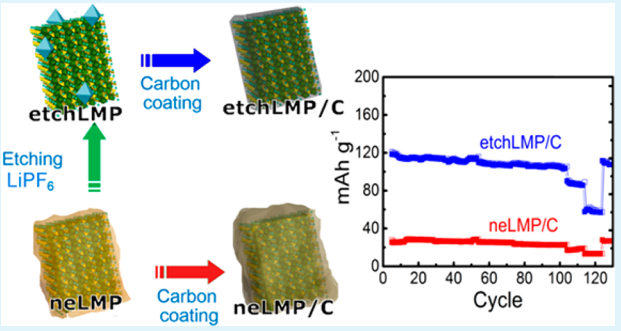


**KEYWORDS:** *Li ion batteries, $LiMnPO_4$, nanocrystals, surface etching, high rate capability*



## INTRODUCTION

Lithium transition metal phosphates with olivine structure have been proposed since almost 20 years[1] as cathode materials for rechargeable lithium-ion batteries, due to their high chemical and thermal stability and the low cost of their precursors. Olivines (orthorhombic space group *Pnma*) are characterized by the presence of longitudinal channels along their crystallographic *b*-axis. These channels are suitable for lithium-ion intercalation and deintercalation reactions that take place during the cathode discharge and charge processes, respectively.[2] The most studied (and now commercially available) olivine is lithium iron phosphate ($LiFePO_4$, LFP) which is characterized by a working potential of 3.45 V vs $Li^+$/Li, with a theoretical capacity of 170 mA h $g^{-1}$. In LFP, the intercalation/deintercalation process is biphasic (from $LiFePO_4$ to $FePO_4$ and *vice versa*) and is reversible. The lithiated and the nonlithiated phases have similar structures, so that the conversion from one phase to the other entails a small volume change, which is indeed desirable for the electrode cycling stability. Among the other olivines, $LiMnPO_4$ (LMP) is more attracting than LFP, since it is has the same theoretical specific capacity as LFP (170 mA h $g^{-1}$), but is characterized by a higher working potential (4.1 V vs $Li^+$/Li). The pervasive use of LMP would enable the development of batteries with energy densities that are approximately 20% higher than those based on LFP.[3,4] However, compared to LFP, LMP is affected by a few additional issues, such as lower delivered capacity and cycling stability, and its poor rate capability. These are related to the low electronic conductivity (about 2 orders of magnitude lower than that of LFP)[5] and the poor $Li^+$ intercalation/deintercalation kinetics. The latter arises from the pseudo Jahn−Teller distortion of the crystal lattice occurring at the interface between $LiMnPO_4$ and $MnPO_4$ during electrode cycling.[4,6,7]

**Received:** November 30, 2015
**Accepted:** January 22, 2016
**Published:** January 22, 2016

  

DOI: 10.1021/acsami.5b11632
*ACS Appl. Mater. Interfaces* 2016, 8, 4069−4075

Many attempts have been made to overcome these limiting factors in olivine type materials for batteries. The poor electronic conductivity is usually improved by carbon coating,[6,8−10] while working with nanosized crystals helps to reduce the $Li^+$ diffusion length[11−17] and consequently improves the ionic conductivity. Beneficial effects on the electrochemical performances are also seen by the incorporation of dopants, such as V,[18] Fe,[19] Ce,[20] Ni,[21] and Mg,[22] that can buffer the pseudo Jahn−Teller distortion. To circumvent the effects of high electronic and ionic resistances, it is customary in the laboratory to adopt charge protocols for the cathode cycling tests (i.e., low currents and long charge times),[23−26] since a slower charging process maximizes the final achievable capacity. These conditions are however far from the realistic case in which an actual battery works and that requires fast charge processes. Only few reports on LMP-based cathodes have adopted fast charge protocols, and all of them based on composite electrode formulations that invariably contain a considerable fraction of carbon and polymeric binder (more than 25% in weight).[14,15,27] Also, carbon was present not only as coating layer but also in the form of additives (e.g., carbon black powders) that were deemed necessary to enhance the electric conductivity. At the cathodic working potentials, both binder and carbon are inactive for $Li^+$ intercalation/deintercalation. Therefore, a mass of the active material that is, at best, only 75% of the total electrode mass, translates into an overall low energy density of the electrode.[28] These figures are far from the 4% wt in total mass of conductive carbon and Polyvinylidene difluoride (PVdF) binder used in commercial electrodes based on active materials different from LFP and LMP.[29]

We developed recently a colloidal synthesis approach to LFP and LMP nanocrystals (NCs) and, for the specific case of LFP, we also set up a subsequent surface treatment and a carbon coating procedure that delivered high performance LFP NCs-based cathodes.[30,31] The treatment consisted in an etching of the NC surface with $LiPF_6$, which removed the organic ligands bound to the surface of the NCs and enabled then the formation of a compact carbon film in the following carbon coating step. Here, we have extended that procedure to LMP NCs which, similarly to the LFP NCs of our previous work,[31] were prepared by a colloidal approach. We compared the performance at room temperature (23 °C) of etched (etchLMP/C) and not etched (neLMP/C) carbon coated $LiMnPO_4$ NCs-based cathodes (Scheme 1), using an electrode formulation with 80% wt. of active material (i.e., LMP) and 20% wt of carbon plus PVdF binder. Data from galvanostatic charge/discharge tests, the cyclic voltammetries (CVs), and electrochemical impedance spectroscopy (EIS) measurements indicated a remarkable improvement of the electrochemical performances of the etched samples tested at high discharge rates (≥1C) and with a reasonable fast charging protocol. The etchLMP/C-based cathodes exhibited an increase of discharge capacity by more than 300% with respect to the not etched samples at 1C. Moreover, our composite electrodes had a higher fraction of active material (80%) with respect to previous reports (75% at best), which contributes to reducing the need of carbon additive and polymeric binder, with a consequent benefit for the future development of high energy density LMP-based cathodes.

**Scheme 1. Synthetic Route to neLMP/C and etchLMP/C NCs**[a]

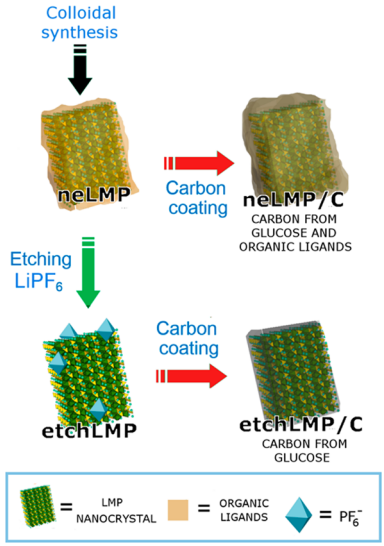


[a]The scheme depicts the procedure used to prepare the neLMP/C particles (top right) by carbon coating of not etched NCs (neLMP, top left) and the etchLMP/C particles (bottom right) by carbon coating of etched NCs (etchLMP, bottom left).

## EXPERIMENTAL METHODS

**Chemicals.** Oleylamine (OAm, 70% purum, LOT#STBF0846 V), 1-octadecene (technical grade, 90%, LOT#MKBS8289 V), manganese chloride anhydrous (99.99% purum), ammonium phosphate dibasic (≥99.0% purum, LOT#BCBD7253 V), lithium iodide (99.99% purum, LOT#MKBN9943 V), α-D-glucose (99.5% purum, LOT#089 K00603), chloroform (99.8% purum, LOT#STBF4628 V), ethanol (99.8% purum, LOT#BCBQ5114 V), *N*-methyl-2-pyrrolidone, polyvinylidene difluoride (PVdF), 1 M $LiPF_6$ electrolyte solution in ethylene carbonate (EC)/dimethylcarbonate (DMC) 1:1 (battery grade), Whatman glass fibers separator (GF/D 0.67 mm thick), and Li metal foils (99.9% purum, Lot#SHBD1554 V) were purchased from Sigma-Aldrich. Coin type 2032 components (SS casing items) were purchased from M.T.I. Corporation. Carbon powder (carbon super P) was purchased from Alfa Aesar.

**Synthesis of $LiMnPO_4$ NCs.** Colloidal LMP NCs were prepared with a procedure that was adapted from our previous reports on LFP NCs:[30,31] 0.90 g of lithium iodide (LiI), 0.63 g of manganese(II) chloride ($MnCl_2$ anhydrous), 0.60 g of ammonium phosphate dibasic ($(NH_4)_2HPO_4$), 50 mL of oleylamine, and 50 mL of 1-octadecene were mixed in a 250 mL three-neck round-bottom flask connected to a standard Schlenk line. The solution was degassed under vacuum for 4 h at 120 °C, after which it was heated overnight at 250 °C (heating rate 5 °C/min) under $N_2$. It was then precipitated and cleaned by repeated additions of chloroform and ethanol followed by centrifugation at 9000 rpm.

**$LiPF_6$ Treatment.** The as-synthesized LMP NCs (500 mg) were dissolved in 10 mL of chloroform and mixed with 10 mL of 0.33 M lithium hexafluorophosphate ($LiPF_6$) aqueous solution. The final 20 mL mixture was vigorously shaken and sonicated for 0.5 h. After 15 min, the $LiMnPO_4$ NCs were transferred into the aqueous phase. The aqueous phase was then collected and centrifuged at 9000 rpm. The precipitate was vigorously shaken in a mixture of ultrapure water (30 mL) and chloroform (20 mL), to remove the excess of $LiPF_6$ and organics from the NCs. After centrifugation at 9000 rpm, the liquid phase was discarded and the precipitate was then redispersed in 20 mL of ultrapure water and 10 mL of ethanol and it was finally centrifuged at 8000 rpm. This last step was repeated twice.

**Carbon Coating of the LMP NCs.** A coating layer of carbon was produced on both etched and not etched LMP NCs, following the


DOI: 10.1021/acsami.5b11632
ACS Appl. Mater. Interfaces 2016, 8, 4069−4075

procedure described below. For the etchLMP sample, about 500 mg of NCs was dispersed in aqueous glucose solution (150 mg of glucose in 5 mL of water), while for neLMP the NCs were solubilized in 5 mL of glucose dispersion in chloroform. The solutions were sonicated for 0.5h and then dried overnight under vacuum at 40 °C. The pyrolytic procedure that produced the carbonaceous coating was the same for both samples. A quartz combustion boat containing the dried mixture (NCs + glucose) was placed in the middle of a tubular furnace under a slightly reducing atmosphere (95% Ar, 5% $H_2$, 50 sccm) and was heated up to 450 °C (5 °C/min), kept at 450 °C for 1 h and then slowly heated to 650 °C (3 °C/min) and kept at 650 °C for 1 h. The furnace was then cooled down to room temperature, while still under $Ar/H_2$ (95/5%) atmosphere.

**X-ray Diffraction (XRD).** X-ray diffraction (XRD) patterns were recorded on a PANalytical Empyrean X-ray diffractometer equipped with a 1.8 kW Cu K$\alpha$ ceramic X-ray tube, PIXcel$^{3D}$ 2 × 2 area detector and operating at 45 kV and 40 mA. The diffraction patterns were collected in air at room temperature using parallel-beam (PB) geometry and symmetric reflection mode. XRD data analysis was carried out using HighScore 4.1 software from PANalytical.

**Thermogravimetric Analysis (TGA).** The synthesized carbon coated NCs (dried powder) were analyzed by TGA to quantify the fraction of carbon content with respect to the inorganic fraction in the NCs. The thermal analysis was performed using a TGA Q500 instrument, from room temperature (RT) to 700 °C (equilibration time 5 min at 30 °C, heating rate 10 °C/min) in air flux.

**Transmission Electron Microscopy (TEM).** Conventional TEM imaging was performed using a JEOL JEM-1011 microscope working at an acceleration voltage of 100 kV. High-resolution TEM (HRTEM) measurements were acquired with a JEOL JEM-2200FS microscope equipped with a Schottky gun working at an acceleration voltage of 200 kV, a CEOS spherical aberration corrector in the objective lens allowing a spatial resolution of 0.9 Å, and an in-column energy Ω-filter.

**Brunauer–Emmett–Teller (BET) Measurements.** Surface area measurements were carried out by nitrogen physisorption at 77 K in a Quantachrome equipment, model autosorb iQ. The specific surface areas were calculated using the multipoint BET model, considering 11 equally spaced points in the $P/P_0$ range of 0.05–0.30. Prior to measurements, the samples (30–500 mg in form of powder) were degassed for at least 3 h at 60 °C under vacuum to eliminate weakly adsorbed species.

**Electrochemical Measurements.** The electrochemical characterization of the etched and not etched NCs, in both cases after carbon coating, was carried out on composite electrodes with the following formulation: 80 wt % of $LiMnPO_4$ NCs, 15 wt % of total carbon (considering both carbon coting and conductive carbon SuperP) and 5 wt % of PVdF. The electrodes were prepared by "doctor blade" deposition of a slurry in *N*-methyl-2-pyrrolidone of the three components on etched aluminum foil used as current collector. Circular electrodes (geometric area of 1.77 $cm^2$) were cut from the dried depositions, pressed and further dried at 120 °C under vacuum for at least 2 h before use. The active material mass loading for the tested electrodes was about 5 mg $cm^{-2}$. Coin-type (2032) electrochemical cells with Li as counter and reference electrode were assembled and sealed in an argon atmosphere drybox ($H_2O$ and $O_2$ < 0.1 ppm). A dried glass fibers membrane (Whatman GF/D) was used as separator, adding 500 $\mu$L of 1 M $LiPF_6$ electrolyte solution in EC:DMC 1:1 (LP30). The electrochemical behavior was tested by galvanostatic charge/discharge, cyclic voltammetries (CVs) at 30 $\mu$V $s^{-1}$, and electrochemical impedance spectroscopy (EIS). The cells were charged using a constant current–constant voltage (CC–CV) protocol, at different currents (i.e., different C-rates: C/10, 1C, 2C, 5C, and 10C considering 1C = 170 mA $g^{-1}_{LMP}$) up to 4.5 V followed by constant voltage step at 4.5 V for 1 h. The cells were then discharged down to 2.5 V at the same C-rate used for the corresponding charge step. EIS runs were performed on fully charged (4.5 V) and fully discharged (2.5 V) cells, in the range 100 kHz to 10 mHz with a perturbation amplitude of 5 mV and 10 points/decade. CVs and galvanostatic charge/discharge tests were carried out on a MPG-2 (BioLogic) potentiostat/galvanostat, while the electrochemical impedance spectra were collected on a PARSTAT 2273 potentiostat/galvanostat. All the measurements were done at room temperature (23 °C). The reported potentials are referred to the Li electrode and the specific capacity data are referred to the mass of the $LiMnPO_4$ in the cathode (not considering carbon coating).

## RESULTS AND DISCUSSION

**Material Characterization.** The $LiMnPO_4$ NCs were prepared via a colloidal method, by modification of the synthesis that we had previously developed for iron-based phosphor-olivine.[30] The synthesis required the use of organic ligands such as oleylamine and octadecene to stabilize the NCs growth and to control their size. At the same time, the presence of these long chain ligands makes the NCs hydrophobic and soluble only in nonpolar or moderately polar solvents (for example chloroform). The hydrophobicity of the NCs represents a serious drawback during the carbon coating procedure, which usually involves the use of an aqueous glucose solution as carbon source:[10] as the NC solution and the glucose solution would not mix, we were forced to use a glucose dispersion in chloroform. The insolubility of glucose in a nonpolar solvent reduces the possibility of formation of a uniform carbon coating around each individual NC as a consequence of the sugar decomposition during the annealing step. In order to make the NCs hydrophilic and therefore allow an adequate mixing with an aqueous glucose solution, the aliphatic surfactants were removed by a postsynthesis step, by treating the NCs with an aqueous $LiPF_6$ solution, following the same etching procedure developed in our previous paper.[31] The activity of $LiPF_6$ as etching agent is due to its reaction with water, which produces in situ hydrofluoric acid, according to the following mechanism:[31,32]

$$LiPF_6 + H_2O \rightarrow LiF + POF_3 + 2HF$$

The generated HF can act as an etchant on the surface of the LMP nanoparticles, by removing the hydrophobic surfactant molecules and replacing them with hydrophilic $PF_6^-$ anions. The choice of $LiPF_6$ was additionally driven by the fact that anhydrous organic solutions of this salt are commonly used as electrolytes for lithium-ion batteries. We additionally tested $Na_3PO_4$ and $(NH_4)_2HPO_4$ as alternative etching agents, but the corresponding electrodes evidenced lower electrochemical performance (see discussion later and also Figure S5 of the Supporting Information), presumably related to the lower efficiency of such agents in removing the original organic ligands, and therefore they were not considered further.

If, from one side, the hydrophilicity of NCs can be crucial to allow a good contact between particles and carbon, on the other it is also important to maintain the nanometer size dimensions of the particles during the heating treatment that is followed to generate the conductive carbon layer (and that is carried out at a temperature of 650 °C). Such harsh conditions can potentially cause partial coalescence of the NCs into bigger particles. In our case, this was prevented by adopting a double step pyrolytic process (see the Experimental Methods for details) and by maintaining the samples at the final temperature of 650 °C for only 1h.

We performed carbon coating on both etched (etchLMP) and not etched (neLMP) $LiMnPO_4$ NCs, to study the effect of the surface treatment step on the electrochemical performances of the LMP-based cathodes. In the case of etchLMP, the only carbon source came from the added glucose, while for neLMP the carbon sources were represented by both glucose and the


DOI: 10.1021/acsami.5b11632
ACS Appl. Mater. Interfaces 2016, 8, 4069–4075

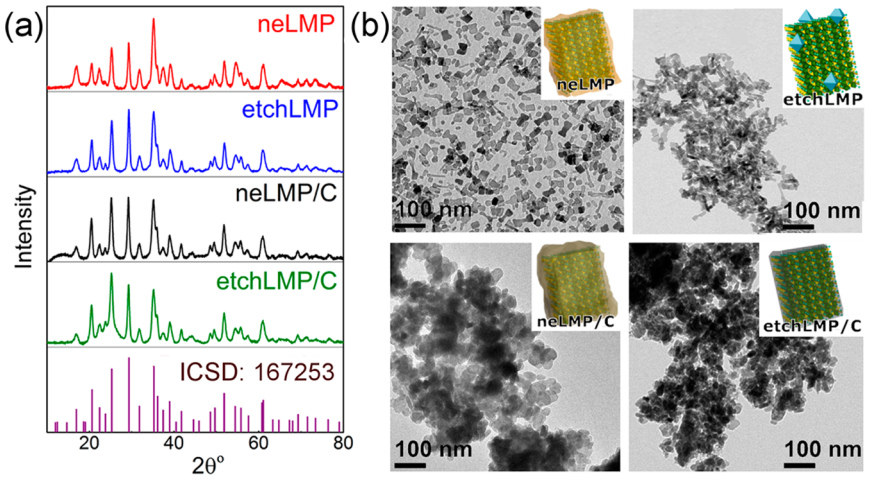


**Figure 1.** Structural and morphological characterization of the not etched and etched $LiMnPO_4$ NCs before (neLMP, etchLMP) and after (neLMP/C, etchLMP/C) carbon coating. (a) XRD patterns corresponding to pure $LiMnPO_4$ with orthorhombic olivine-type structure (ICSD collection code: 167253). (b) Low-magnification TEM images, in which several $LiMnPO_4$ nanoparticles can be seen.

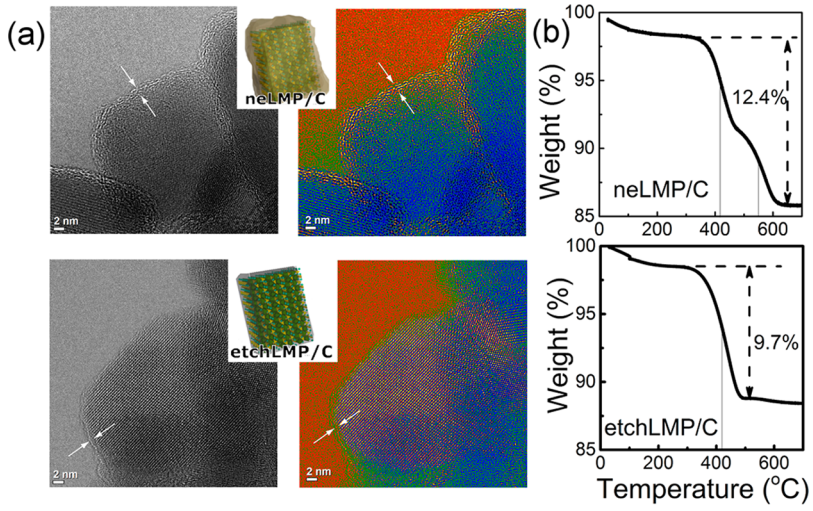


**Figure 2.** Characterization of carbon coating on neLMP/C and etchLMP/C NCs. (a) HRTEM images: the arrows and the different colors evidenced the amorfous carbon layer on neLMP/C NCs and etchLMP/C NCs. (b) TGA analysis of dried powders: the vertical solid lines identify the decomposition temperatures of the carbonaceous layers.

organic ligands coming from the synthesis. The X-ray diffraction (XRD) spectra of the neLMP, etchLMP, neLMP/C and etchLMP/C dry powders are reported in Figure 1a. All samples were characterized by similar diffraction patterns, corresponding to pure $LiMnPO_4$ with orthorhombic olivine-type structure (*Pnma* space group; ICSD collection code: 167253). From the XRD spectra, we can conclude that neither structural changes in the crystals nor impurities were generated during both etching and carbon coating.

TEM images of the initial neLMP, as well as the etchLMP, neLMP/C and etchLMP/C samples are reported in Figure 1b. The initial neLMP NCs exhibited dumbbell and platelet-like shapes, with sizes ranging from few nm to 50 nm, and a specific surface area of 47 $m^2\ g^{-1}$. On average, the lateral size of the NC decreased by about 5−10% after the $LiPF_6$ treatment, which is beneficial as it helps to reduce the $Li^+$ diffusion length. Moreover, the etchLMP showed an increased surface area of 119 $m^2\ g^{-1}$, confirming what we had previously observed on a similar treatment on LFP NCs.[31] The difference in size between the not etched and the etched NCs was retained after the respective samples were carbon coated, even though the carbon coating caused some reshaping and agglomeration of the NCs. The extent of agglomeration was actually minimized by the pyrolytic protocol adopted here. For comparison, the TEM image of Figure S1a, which is referred to etchLMP/C prepared by a simplest single step pyrolytic process at 650 °C (onestep-etchLMP/C), indicates that these particles are clearly bigger than the initial particles, with sizes exceeding 100 nm.

The carbon coated neLMP/C and etchLMP/C NCs were analyzed by HRTEM (Figure 2a). Both samples were characterized by an amorphous carbon layer surrounding the crystals, with the preservation of the platelet morphology. The etched NCs appeared to have a thinner carbon layer than the not etched ones, for which the coating was almost 2.0 nm thick, as evidenced from the fringes at the edges of the particles. To assess the weight fraction in the NCs due to the carbon coating, the neLMP/C and etchLMP/C samples were subjected to TGA analysis under air.[26,33] The data are reported in Figure 2b as percentage of weight loss vs temperature. The two samples exhibited a weight loss in the 300−600 °C range: here, the loss


DOI: 10.1021/acsami.5b11632
ACS Appl. Mater. Interfaces 2016, 8, 4069−4075

of weight coincides with the carbon coating that was converted in $CO_2$, while the residual weight corresponds to $LiMnPO_4$, which is stable even at temperatures above 700 °C. The carbon content was found to be 12.4% wt. for neLMP/C and 9.7% wt. for etchLMP/C. Also, while the TGA curve of the etchLMP/C sample exhibited one step, with a decomposition temperature of 420 °C, the curve of the neLMP/C sample exhibited two steps, with decomposition temperatures of 420 and 570 °C. Since in the etched sample the only carbon source comes from glucose, we assign the lower temperature step in the two samples to the decomposition of the carbon originating from glucose, while the higher temperature step that was seen only in the neLMP/C sample should have arisen from the pyrolysis of carbon originating from the surfactant shell (made of oleylamine and octadecene).

**Electrochemical Performance.** As preliminary electrochemical test, we investigated the behavior of the etchLMP/C and neLMP/C NCs by CVs. Figure 3a compares the CVs

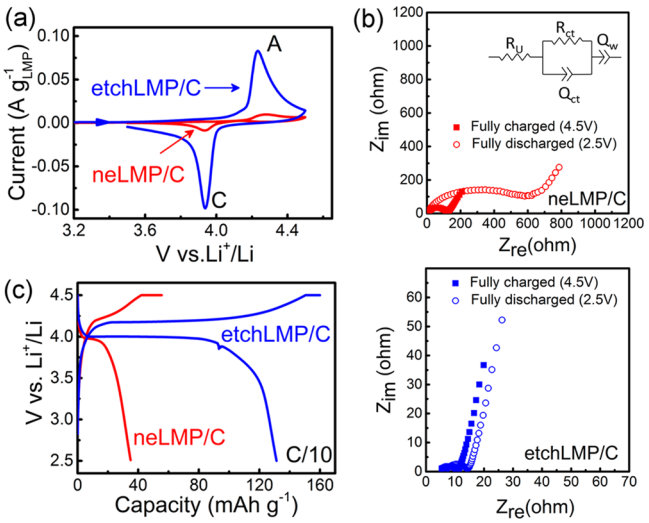


**Figure 3.** Electrochemical characterization of neLMP/C and etchLMP/C-based cells. (a) Cyclic voltammetry performed at scan rate of 30 $\mu$V s$^{-1}$ in the 3.5−4.5 voltage range with current normalized to the active material mass. (b) Electrochemical impedance spectra (Nyquist plot) of the fully charged (4.5 V, full squares) and discharged (2.5 V, empty dots) cells. Inset: scheme of the equivalent circuit that better fits the impedance data of the fully charged cells. (c) Voltage profiles upon the first galvanostatic charge/discharge cycle at C-rate of C/10.

(normalized to the mass of active material) of the two systems. Both samples were characterized by an anodic peak A at 4.23 V which is related to $Mn^{2+}/Mn^{3+}$ oxidation, and a cathodic peak C at 3.93 V attributed to the reverse redox process. The main difference between the two systems is that the value of the normalized current of the peaks for the etched sample (blue line) was almost 8 times higher than that of the neLMP/C (red line). This behavior can indicate a superior conductivity of the former electrode.

To support our assumption we performed EIS of fully charged (4.5 V) and fully discharged (2.5 V) cells. Figure 3b reports the recorded impedance. As expected for a lithium ion battery, the impedance was found to be sensitive to the state of charge of the battery; in particular, it increases in the discharged state because at 2.5 V no redox process takes place, with the consequent enhancement of charge transfer resistance.[34] The equivalent circuit that better fits the EIS data of the fully charged cells (see Figure 3b inset) is composed by an uncompensated resistance ($R_U$) in series with one parallel $R_{ct}/Q_{ct}$ and $Q_W$ elements, with $R_{ct}$ and $Q_{ct}$ corresponding to charge transfer resistance and constant phase element respectively, $Q_W$ corresponding to a constant phase element related to $Li^+$ diffusion. From the fitting of the experimental data, the extrapolated $R_{ct}$ for the neLMP/C is ~212 Ω cm$^2$ while $R_{ct}$ for the etchLMP/C is almost 18 times lower (i.e., 12 Ω cm$^2$). The lower $R_{ct}$ value for the etched sample is in good agreement with the CVs data and represents a clear evidence of the higher conductivity achieved by etching the NCs prior to carbon coating. Therefore, etching does improve the quality of the carbon coating that is grown on the particles. From the data in the lower frequency range (the so-called Warburg region) using eqs 1 and 2, it is possible to estimate the ratio between the $Li^+$ diffusion coefficients ($D_{Li+}$) for the etched and not etched samples:[35,36]

$$\frac{D_{\mathrm{Li}_{\mathrm{etchLMP/C}}}}{D_{\mathrm{Li}_{\mathrm{neLMP/C}}}} = \left(\frac{\sigma_{\mathrm{neLMP/C}}}{\sigma_{\mathrm{etchLMP/C}}}\right)^2 \quad (1)$$

$$D_{\mathrm{Li}} = \frac{R^2T^2}{n^4F^4A^2C^2\sigma^2} \quad (2)$$

where $R$ is the Regnault gas constant, $T$ is the absolute temperature, $n$ is the number of electrons transferred in the redox process, $F$ is the Faraday constant, $A$ is the surface area of the LMP-based electrode, $C$ is the $Li^+$ concentration in the solid electrode, and $\sigma$ is the Warburg factor. The Warburg factors $\sigma$ were determined from the plot (Figure S2) of the real components of the impedance ($Z_{Re}$) versus the reciprocal of the square root of the angular frequency ($\omega^{-1/2}$), according to the following expression:[35,36]

$$Z_{\mathrm{Re}} = R_{ct} + R_s + \sigma\omega^{-1/2} \quad (3)$$

The estimated $D_{Li}$ ratio reveals that the $Li^+$ diffusion is almost 2 orders of magnitude faster in the case of etchLMP/C compared to the neLMP/C. This remarkable result further confirms the critical role of NC surface etching: this step not only improves the electron conductivity, but it positively affects the $Li^+$ diffusion rate.

The electrochemical behavior of the etched and not etched LMP/C-based cells was finally studied by galvanostatic charge/discharge cycles. Figure 3c compares the first voltage profiles upon galvanostatic charge/discharge at the low C-rate of C/10 of the two studied LMP samples. The etchLMP/C-based electrode delivered a specific capacity around 130 mA h g$^{-1}$, while the not etched sample exhibited a poor capacity of only 35 mA h g$^{-1}$. Already since these first charge/discharge cycles, the superior performance of the etchLMP/C sample was clearly visible. In view of actual exploitation in a real battery scenario, we studied the etchLMP/C-based cathodes at different charge and discharge C-rates, ranging from 1C to 10C, with particular attention to the charge process. The adopted charge protocol (see the Experimental Methods for details) enabled a reasonable fast charge time of maximum 2h at 1C-rate, and even faster at higher C-rates. Figure 4 reports the specific capacity and the recovered charge vs cycle number (a) and the corresponding voltage profiles for the first charge/discharge cycle (b) at each tested C-rates for etchLMP/C sample. For comparison, Figure 4a reports in addition the specific capacity


DOI: 10.1021/acsami.5b11632
ACS Appl. Mater. Interfaces 2016, 8, 4069−4075

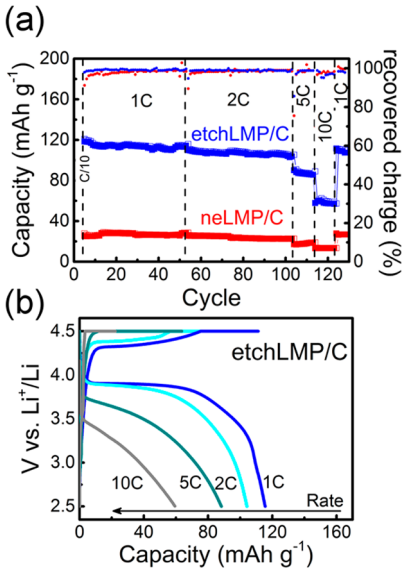


**Figure 4.** Galvanostatic charge/discharge performances at discharge rates of 1C, 2C, 5C, and 10C. The electrodes were charged following a constant current−constant voltage protocol. (a) Comparison of specific capacity (mA h $g^{-1}$) and recovered charge (%) vs cycle number for etchLMP/C and neLMP/C−based electrodes. (b) Voltage profiles upon the first galvanostatic charge/discharge cycle for etchLMP/C-based electrode.

of the neLMP/C-based cell, while the voltage profiles for the first charge/discharge cycle are reported in Figure S3.

The etchLMP/C electrode exhibited a specific capacity of 118 mA h $g^{-1}$ at 1C with a stable cycling performance, with a capacity fade of 0.06% per cycle during the first 50 cycles. At 2C, 5C, and 10C, the capacities were 110, 90, and 60 mA h $g^{-1}$, respectively. The etchLMP/C delivered capacity was higher than that of the neLMP/C NCs, which never exceeded 30 mA $g^{-1}$ at all tested C-rates. At the end of the whole charge/discharge protocol (120 cycles at different C-rates), the etchLMP/C electrode delivered, at 1C, a capacity of 109 mA h $g^{-1}$. This value corresponds to 92% of the initial capacity. When a slower charge protocol (i.e., charging constant voltage times of 10 h) was adopted, the etchLMP/C-based cathode showed a specific capacity increase of about 14% at both C/10 an 1C (Figure S4) with respect to the data reported in Figure 4. However, even if slow charge protocols are a common practice in the literature[23−26] and allow higher discharge capacity values, the cell performances are far from what is required for a practical use of a battery that usually needs fast charge processes. The good rate capability of etchLMP/C NCs, compared to the not etched sample can be primarily related to a better and more effective carbon coating on the NCs surface. As mentioned earlier, other etching agents, such as $Na_3PO_4$ and $(NH_4)_2HPO_4$, were tested, but the electrochemical results (Figure S5) confirmed the superior performance of LMP sample treated with $LiPF_6$. Clearly, the high cost of $LiPF_6$ and the in situ formation of toxic HF in such treatment represent important concerns. Therefore, further research will be devoted to identify a much cheaper and less toxic etching agent. The rate capability here reported for the etchLMP/C NCs represents an important result, taking into account the electrode formulation (80% wt. active material) and the adopted charge protocol.

## CONCLUSION

In summary, we have prepared $LiMnPO_4$ nanocrystals through colloidal synthesis, followed by surface etching with $LiPF_6$ and carbon coating with glucose. We demonstrate the crucial and beneficial effect of the postsynthesis etching procedure on the electrochemical performances of so-prepared etchLMP/C-based cathodes for LIBs. The aforementioned electrodes showed good and stable electrochemical performances, displaying discharge capacities at 1C of 118 mA h $g^{-1}$, 4 times higher than those of electrodes based on not etched LMP/C. The favorable influences of the adopted etching process are as follows: (i) The efficient removal of the hydrophobic passivated surfactants shell, present on NCs surface after the colloidal synthesis. This increases the nanoparticles' solubility in the aqueous glucose solution used as carbon source for NCs coating, enabling the formation of a good conductive carbon layer. (ii) The possibility to prepare composite electrodes with a reduced amount of carbon additive and polymeric binder, with a consequent benefit on the energy density of LMP-based cathodes. The protocol reported here enabled the preparation of LMP/NCs-based cathodes with high rate capability and which can be charged with a reasonable fast CC−CV procedure (of maximum 2 h at 1C-rate), which is of paramount importance for the future development of high rate and high power Li-ion batteries.

## ASSOCIATED CONTENT

### Supporting Information

The Supporting Information is available free of charge on the ACS Publications website at DOI: 10.1021/acsami.5b11632.

Role of the pyrolysis protocol on the NCs size, impedance analysis: evaluation of Warburg factors ($\sigma$), additional details on the electrochemical performances and electrochemical test with alternative etching agents (PDF)

## AUTHOR INFORMATION

### Corresponding Authors

*E-mail: liberato.manna@iit.it.

*E-mail: simone.monaco@iit.it.

### Author Contributions

The manuscript was written through contributions of all authors. All authors have given approval to the final version of the manuscript.

### Notes

The authors declare no competing financial interest.

## ACKNOWLEDGMENTS

The research leading to these results was supported by the European Union through the FP7 consolidator ERC Grant "TRANS-NANO" (Contract No. 614897).

## REFERENCES

(1) Padhi, A. K.; Nanjundaswamy, K. S.; Goodenough, J. B. Phospho-Olivines as Positive-Electrode Materials for Rechargeable Lithium Batteries. *J. Electrochem. Soc.* **1997**, *144*, 1188−1194.

(2) Alyoshin, V. A.; Pleshakov, E. A.; Ehrenberg, H.; Mikhailova, D. Platelike $LiMPO_4$ (M = Fe, Mn, Co, Ni) for Possible Application in Rechargeable Li Ion Batteries: Beyond Nanosize. *J. Phys. Chem. C* **2014**, *118*, 17426−17435.

(3) Delacourt, C.; Laffont, L.; Bouchet, R.; Wurm, C.; Leriche, J. B.; Morcrette, M.; Tarascon, J. M.; Masquelier, C. Toward Understanding



DOI: 10.1021/acsami.5b11632
*ACS Appl. Mater. Interfaces* 2016, 8, 4069−4075

of Electrical Limitations (Electronic, Ionic) in $LiMPO_4$ (M = Fe, Mn) Electrode Materials. *J. Electrochem. Soc.* **2005**, *152*, A913−A921.
(4) Wang, D. Y.; Buqa, H.; Crouzet, M.; Deghenghi, G.; Drezen, T.; Exnar, I.; Kwon, N. H.; Miners, J. H.; Poletto, L.; Graetzel, M. High-Performance, Nano-Structured $LiMnPO_4$ Synthesized Via a Polyol Method. *J. Power Sources* **2009**, *189*, 624−628.
(5) Yonemura, M.; Yamada, A.; Takei, Y.; Sonoyama, N.; Kanno, R. Comparative Kinetic Study of Olivine $Li_xMPO_4$ (M = Fe, Mn). *J. Electrochem. Soc.* **2004**, *151*, A1352−A1356.
(6) Dong, Y. Z.; Wang, L.; Zhang, S. L.; Zhao, Y. M.; Zhou, J. P.; Xie, H.; Goodenough, J. B. Two-Phase Interface in $LiMnPO_4$ Nanoplates. *J. Power Sources* **2012**, *215*, 116−121.
(7) Piper, L. F. J.; Quackenbush, N. F.; Sallis, S.; Scanlon, D. O.; Watson, G. W.; Nam, K. W.; Yang, X. Q.; Smith, K. E.; Omenya, F.; Chernova, N. A.; Whittingham, M. S. Elucidating the Nature of Pseudo Jahn-Teller Distortions in $Li_xMnPO_4$: Combining Density Functional Theory with Soft and Hard X-Ray Spectroscopy. *J. Phys. Chem. C* **2013**, *117*, 10383−10396.
(8) Bakenov, Z.; Taniguchi, I. Physical and Electrochemical Properties of $LiMnPO_4$/C Composite Cathode Prepared with Different Conductive Carbons. *J. Power Sources* **2010**, *195*, 7445−7451.
(9) Oh, S. M.; Oh, S. W.; Myung, S. T.; Lee, S. M.; Sun, Y. K. The Effects of Calcination Temperature on the Electrochemical Performance of $LiMnPO_4$ Prepared by Ultrasonic Spray Pyrolysis. *J. Alloys Compd.* **2010**, *506*, 372−376.
(10) Wang, J. J.; Sun, X. L. Understanding and Recent Development of Carbon Coating on $LiFePO_4$ Cathode Materials for Lithium-Ion Batteries. *Energy Environ. Sci.* **2012**, *5*, 5163−5185.
(11) Bakenov, Z.; Taniguchi, I. Electrochemical Performance of Nanocomposite $LiMnPO_4$/C Cathode Materials for Lithium Batteries. *Electrochem. Commun.* **2010**, *12*, 75−78.
(12) Xiao, J.; Xu, W.; Choi, D. W.; Zhang, J. G. Synthesis and Characterization of Lithium Manganese Phosphate by a Precipitation Method. *J. Electrochem. Soc.* **2010**, *157*, A142−A147.
(13) Rui, X. H.; Zhao, X. X.; Lu, Z. Y.; Tan, H. T.; Sim, D. H.; Hng, H. H.; Yazami, R.; Lim, T. M.; Yan, Q. Y. Olivine-Type Nanosheets for Lithium Ion Battery Cathodes. *ACS Nano* **2013**, *7*, 5637−5646.
(14) Zhang, W. X.; Shan, Z. Q.; Zhu, K. L.; Liu, S. Z.; Liu, X. Y.; Tian, J. H. $LiMnPO_4$ Nanoplates Grown Via a Facile Surfactant-Mediated Solvothermal Reaction for High-Performance Li-Ion Batteries. *Electrochim. Acta* **2015**, *153*, 385−392.
(15) Guo, H.; Wu, C. Y.; Xie, J.; Zhang, S. C.; Cao, G. S.; Zhao, X. B. Controllable Synthesis of High-Performance $LiMnPO_4$ Nanocrystals by a Facile One-Spot Solvothermal Process. *J. Mater. Chem. A* **2014**, *2*, 10581−10588.
(16) Wang, G. X.; Liu, H.; Liu, J.; Qiao, S. Z.; Lu, G. Q. M.; Munroe, P.; Ahn, H. Mesoporous $LiFePO_4$/C Nanocomposite Cathode Materials for High Power Lithium Ion Batteries with Superior Performance. *Adv. Mater.* **2010**, *22*, 4944−4948.
(17) Kretschmer, K.; Sun, B.; Su, D.; Zhao, Y.; Wang, G. Scalable Preparation of $LiFePO_4$/C Nanocomposites with $sp^2$-Coordinated Carbon Coating as High-Performance Cathode Materials for Lithium-Ion Batteries. *ChemElectroChem* **2015**, *2*, 2096−2103.
(18) Gutierrez, A.; Qiao, R. M.; Wang, L. P.; Yang, W. L.; Wang, F.; Manthiram, A. High-Capacity, Aliovalently Doped Olivine $LiMn_{(1-3x/2)}V_{x\ \mathrm{Square}\ x/2}PO_4$ Cathodes without Carbon Coating. *Chem. Mater.* **2014**, *26*, 3018−3026.
(19) Zhang, K.; Han, X. P.; Hu, Z.; Zhang, X. L.; Tao, Z. L.; Chen, J. Nanostructured Mn-Based Oxides for Electrochemical Energy Storage and Conversion. *Chem. Soc. Rev.* **2015**, *44*, 699−728.
(20) Kou, L. Q.; Chen, F. J.; Tao, F.; Dong, Y.; Chen, L. High Rate Capability and Cycle Performance of Ce-Doped $LiMnPO_4$/C Via an Efficient Solvothermal Synthesis in Water/Diethylene Glycol System. *Electrochim. Acta* **2015**, *173*, 721−727.
(21) Iturrondobeitia, A.; Goni, A.; Gil de Muro, I. G.; Lezama, L.; Kim, C.; Doeff, M.; Cabana, J.; Rojo, T. High-Voltage Cathode Materials for Lithium-Ion Batteries: Freeze-Dried $LiMn_{0.8}Fe_{0.1}M_{0.1}PO_4$/C (M = Fe, Co, Ni, Cu) Nanocomposites. *Inorg. Chem.* **2015**, *54*, 2671−2678.
(22) Omenya, F.; Miller, J. K.; Fang, J.; Wen, B. H.; Zhang, R. B.; Wang, Q.; Chernova, N. A.; Whittingham, M. S. Single-Phase Lithiation and Delithiation of Simferite Compounds Li(Mg,Mn,Fe)-$PO_4$. *Chem. Mater.* **2014**, *26*, 6206−6212.
(23) Cheng, G. Y.; Zuo, P. J.; Wang, L. G.; Shi, W.; Ma, Y. L.; Du, C. Y.; Cheng, X. Q.; Gao, Y. Z.; Yin, G. P. High-Performance Carbon-Coated Limnpo4 Nanocomposites by Facile Two-Step Solid-State Synthesis for Lithium-Ion Battery. *J. Solid State Electrochem.* **2015**, *19*, 281−288.
(24) Xia, Q. B.; Liu, T.; Xu, J. J.; Cheng, X. Y.; Lu, W.; Wu, X. D. High Performance Porous $LiMnPO_4$ Nanoflakes: Synthesis from a Novel Nanosheet Precursor. *J. Mater. Chem. A* **2015**, *3*, 6301−6305.
(25) Zhao, M.; Fu, Y.; Xu, N.; Li, G. R.; Wu, M. T.; Gao, X. P. High Performance $LiMnPO_4$/C Prepared by a Crystallite Size Control Method. *J. Mater. Chem. A* **2014**, *2*, 15070−15077.
(26) Zhang, L. F.; Qu, Q. T.; Zhang, L.; Li, J.; Zheng, H. H. Confined Synthesis of Hierarchical Structured $LiMnPO_4$/C Granules by a Facile Surfactant-Assisted Solid-State Method for High-Performance Lithium-Ion Batteries. *J. Mater. Chem. A* **2014**, *2*, 711−719.
(27) Su, J.; Liu, Z. Z.; Long, Y. F.; Yao, H.; Lv, X. Y.; Wen, Y. X. Enhanced Electrochemical Performance of $LiMnPO_4$/C Prepared by Microwave-Assisted Solvothermal Method. *Electrochim. Acta* **2015**, *173*, 559−565.
(28) Varzi, A.; Taubert, C.; Wohlfahrt-Mehrens, M.; Kreis, M.; Schutz, W. Study of Multi-Walled Carbon Nanotubes for Lithium-Ion Battery Electrodes. *J. Power Sources* **2011**, *196*, 3303−3309.
(29) Marks, T.; Trussler, S.; Smith, A. J.; Xiong, D. J.; Dahn, J. R. A Guide to Li-Ion Coin-Cell Electrode Making for Academic Researchers. *J. Electrochem. Soc.* **2011**, *158*, A51−A57.
(30) Paolella, A.; Bertoni, G.; Dilena, E.; Marras, S.; Ansaldo, A.; Manna, L.; George, C. Redox Centers Evolution in Phospho-Olivine Type ($LiFe_{0.5}Mn_{0.5}PO_4$) Nanoplatelets with Uniform Cation Distribution. *Nano Lett.* **2014**, *14*, 1477−1483.
(31) Paolella, A.; Bertoni, G.; Marras, S.; Dilena, E.; Colombo, M.; Prato, M.; Riedinger, A.; Povia, M.; Ansaldo, A.; Zaghib, K.; Manna, L.; George, C. Etched Colloidal $LiFePO_4$ Nanoplatelets toward High-Rate Capable Li-Ion Battery Electrodes. *Nano Lett.* **2014**, *14*, 6828−6835.
(32) Barlowz, C. G. Reaction of Water with Hexafluorophosphates and with Li Bis(Perfluoroethylsulfonyl)Imide Salt. *Electrochem. Solid-State Lett.* **1999**, *2*, 362−364.
(33) Damen, L.; De Giorgio, F.; Monaco, S.; Veronesi, F.; Mastragostino, M. Synthesis and Characterization of Carbon-Coated $LiMnPO_4$ and $LiMn_{1-X}Fe_xPO_4$ (X = 0.2, 0.3) Materials for Lithium-Ion Batteries. *J. Power Sources* **2012**, *218*, 250−253.
(34) Rodrigues, S.; Munichandraiah, N.; Shukla, A. K. A Review of State-of-Charge Indication of Batteries by Means of A.C. Impedance Measurements. *J. Power Sources* **2000**, *87*, 12−20.
(35) Zhang, Z. H.; Zhou, Z. F.; Nie, S.; Wang, H. H.; Peng, H. R.; Li, G. C.; Chen, K. Z. Flower-Like Hydrogenated $TiO_2$(B) Nanostructures as Anode Materials for High-Performance Lithium Ion Batteries. *J. Power Sources* **2014**, *267*, 388−393.
(36) Bard, A. J.; Faulkner, L. R. *Electrochemical Methods: Fundamentals and Applications*, 2nd ed.; Wiley: New York, 2001; 833 pp.


DOI: 10.1021/acsami.5b11632
*ACS Appl. Mater. Interfaces* 2016, 8, 4069−4075